Determination of Pressure Coefficients for High-Rise Buildings of Different Aspect Ratios

Final Report

Structural Engineering Institute of ASCE

Donald R. Scott, S.E., F.SEI, F.ASCE
Gregory A. Kopp, Ph.D., P.E., M.ASCE
Jin Wang
Laura Champion, P.E., F.SEI, M.ASCE
Jennifer Goupil, P.E., F.SEI, M.ASCE

Sponsored by:
The Charles Pankow Foundation

March 27, 2020

Determination of Pressure Coefficients for High-Rise Buildings of Different Aspect Ratios

CPF Research Grant Agreement #04-19

Funded by
CHARLES PANKOW FOUNDATION
1390 Chain Bridge Road, Suite 700
McLean, Virginia 22101-3904

Team - Principal Investigator:	Donald R. Scott, S.E., F.SEI, F.ASCE
Team – Technical Lead:	Gregory A. Kopp, Ph.D., P.E., M.ASCE Jin Wang
Team – SEI:	Laura Champion, P.E., F.SEI, M.ASCE Jennifer Goupil, P.E., F.SEI, M.ASCE

Acknowledgements

This project was made possible by funding from the Charles Pankow Foundation, and the following co-funders:

- Walter P Moore and Associates, Inc.
- Skidmore, Owings & Merrill
- PCS Structural Solutions
- National Council of Structural Engineers Associations
- Glenn and Judy Bell
- CPP WIND ENGINEERING & AIR QUALITY CONSULTANTS
- Peter A. Irwin, Ph.D., P.Eng.
- Degenkolb Engineers
- Gilsanz Murray Steficek LLP
- Hatfield Group
- KPFF
- LERA Consulting Structural Engineers
- Magnusson Klemencic Associates Foundation
- NABIH YOUSSEF STRUCTURAL ENGINEERS
- Odeh Engineers, Inc.
- Silman
- Structural Focus.

Pressure Coefficients Measurements of Mid- and High-Rise Buildings with Different Aspect Ratios

Gregory A. Kopp, Jin Wang
Boundary Layer Wind Tunnel Laboratory, Faculty of Engineering
University of Western Ontario, London, ON, Canada

1. BACKGROUND

The pressure coefficients for the Main Wind Force Resisting System (MWFRS) in Chapter 27 of ASCE 7-16 for buildings above 60ft date from the mid-1970s, primarily from the work of Akins et al. (1977). While tweaks to them have been made over the years, a systematic study using modern wind tunnel test methods for code-based design has not been conducted in many years. In particular, our knowledge of both the role of turbulence on aerodynamic loading and the turbulence levels in the atmospheric boundary later have evolved considerably over this time period. As a result, the ASCE 7-22 Wind Loads Sub-Committee wishes to review and possibly update Chapter 27 MWFRS wind load coefficients.

The University of Western Ontario (UWO) has been re-visiting the design pressure coefficients, which has led to a large database of aerodynamic loads for buildings with many different building plan and height aspect ratios (Ho et al, 2005; Liu et al., 2019), where the plan aspect ratio is ratio of the two plan dimensions while height ratio is defined as the height of the building relative to the least horizontal dimension. The UWO database has a gap in height ratios between the low-rise (Ho et al., 2005) and the high-rise (Liu et al., 2019) buildings. Thus, the complete generality of the results is not resolved. The objective of this study was to obtain additional test data so as to provide information for height aspect ratios to provide a complete set of data for analysis of the provisions of ASCE 7.

2. EXPERIMENTAL SETUP

The experiments were carried out in the high-speed test section of the closed-return Boundary-Layer Wind Tunnel II at UWO. The high-speed test section is 3.4m wide, 2.1m high with a 30m long inlet to the center of the turntable. The maximum wind speed is 30m/s. The wind tunnel floor has a fully automated surface roughness elements, with blocks that have a maximum height of 200mm, to generate the desired boundary layer characteristics. For the present study, we focus on the tests in an open exposure (Terrain Category C).

2.1 Wind simulation

Wind speeds were measured by using a Cobra Probe (TFI, Model No. 900) at a sampling frequency of 625Hz. The measured wind field is presented in Fig. 1. The wind speed and turbulence profiles fit well with the ESDU model for z_o=0.034m (full-scale). The power law profile has an exponent of 0.12, which is an open country exposure. In addition, Fig. 1b shows the fit of the measured stream wise velocity spectrum and the von Karman spectrum at an equivalent full-scale height, z=96m.

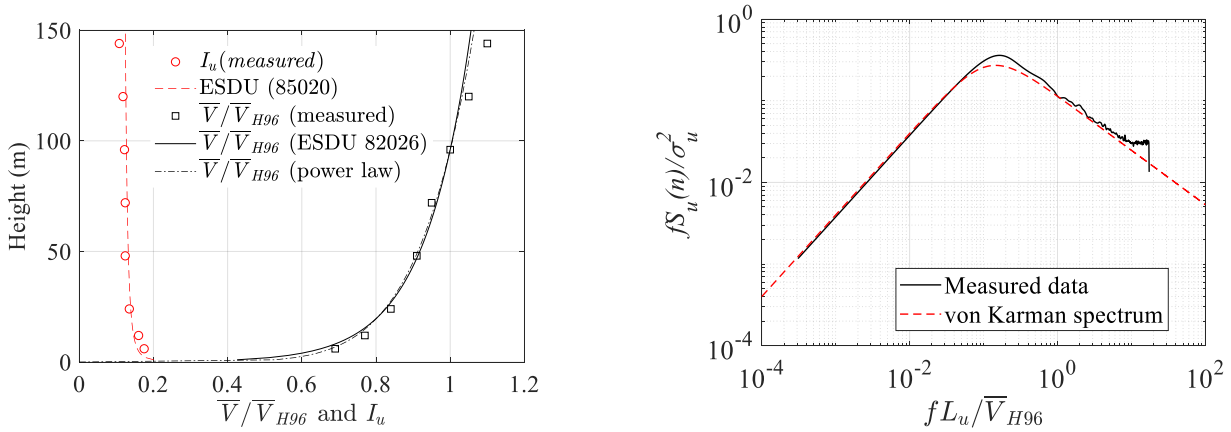

(a) (b)

Fig. 1 Wind speed profile and spectrum: (a)Wind speed profile; (b)Velocity spectrum.

2.2 Building models

The models for the pressure tests were made by the University Machine Services at the University of Western Ontario. A group of rectangular-plan building models, a total of 30, were tested in the wind tunnel. Table 1 shows the configurations of the tested buildings. Generally, the models are categorized into 5 groups, each with the same roof height. The plan aspect ratios vary from 1 to 4, and the height-to-width ratios range from 1 to 12. Fig. 2a illustrates the tested building models. The model numbers in the figures correspond to those in Table 1. The length scale of the models is 1/100 for the models with height-to-width ratios of 1 and 2. Otherwise, it is 1/200 for the remaining higher models. The length, L, and breadth, B, are defined based on the wind direction, as Chapter 27 states, in which L is the horizontal plan dimension parallel to wind direction and B is the dimension normal to wind direction, as shown in Fig. 2b. The previous high-rise building models in Liu and Kopp (2019), and TPU aerodynamic database, does not consider the roof pressures. In our present study, all the models were machined with pressure taps distributed on the roof and walls. The number of pressure taps set on the building models are given in Table 1.

The pressure measurements were conducted for wind directions varying from 10° to 90°, with 10° increment. The sampling duration is 180 seconds, with the sampling frequency of 625Hz for

wind field measurements. The output of the measurement is a set of pressure time series from each tap location, referenced to the dynamic velocity pressure measured at a 1.47m in the wind tunnel where the flow is uniform with low turbulence level. Therefore, all the data need to be re-referenced to the mean roof height dynamic pressure by the ratio of dynamic pressure at upper level and the dynamic pressure at mean roof height.

Table 1. Summary of the building geometries

Building No.	Width W (m) (full-scale)	Depth D (m) (full-scale)	Roof height H (m) (full-scale)	Height-to-width ratio (H/W)	Length scale	Pressure taps number
1	12	48	12	4	1:100	305
2		36		3		260
3		30		2.5		230
4		24		2		200
5		18		1.5		170
6		12		1		140
7	12	48	24	4	1:100	525
8		36		3		450
9		30		2.5		400
10		24		2		350
11		18		1.5		300
12		12		1		250
13	12	48	48	4	1:200	264
14		36		3		212
15		30		2.5		186
16		24		2		160
17		18		1.5		134
18		12		1		108
19	12	48	96	4	1:200	444
20		36		3		356
21		30		2.5		312
22		24		2		268
23		18		1.5		224
24		12		1		180
25	12	48	144	4	1:200	390
26		36		3		320
27		30		2.5		294
28		24		2		250
29		18		1.5		224
30		12		1		180

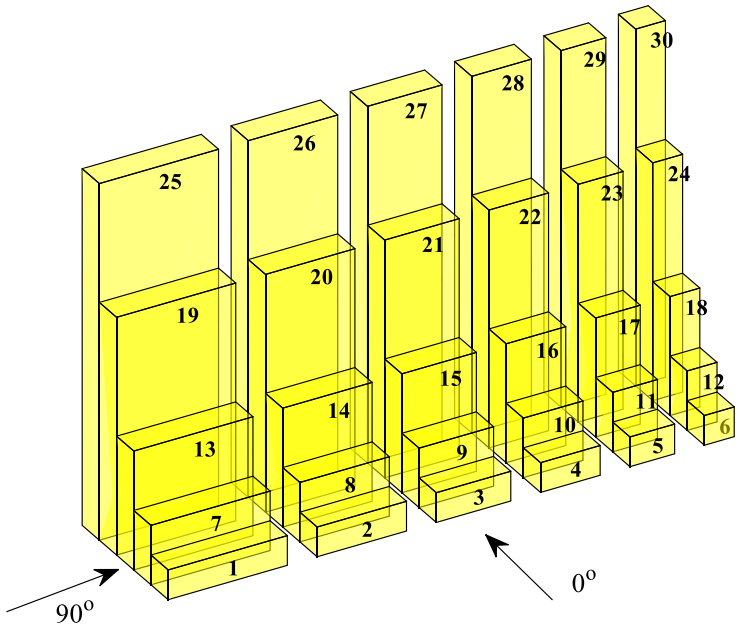

(a)

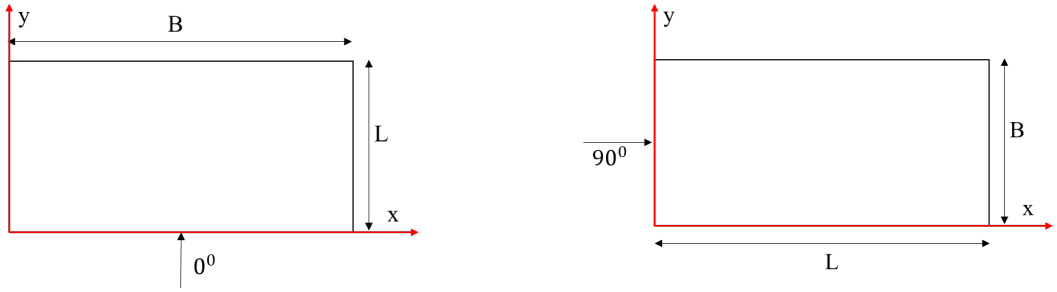

(b)

Fig. 2 Building models tested at UWO: (a) Building model configurations; (b) Definitions of length, L, and breadth, B

3. RESULTS AND DISCUSSION

In this complete study, we are focussing primarily on the overall uplift, base shear coefficients and gust-effect factor for the complete data set of about 70 building shapes. In addition, the area-averaged wall pressure coefficients will be analyzed. Both the mean and peak values, i.e., Cp and [GCp] corresponding to those of Chapters 27, 28 and 30 in ASCE 7-16, are being investigated. For the present report, we are providing a sample of initial results, focusing on the two orthogonal wind directions of 0° and 90°, for simplicity. The complete analysis and investigation based on the measured data are still in process and will be presented in a subsequent report, which integrates

the current data with those of Ho et al. (2005), Liu et al. (2019), along with recommendations for ASCE 7-22.

3.1 Overall uplift

Fig. 3 shows the mean and peak uplift coefficients for each building, for the two wind directions. In addition, the net uplift coefficients as determined by Chapter 27 are included, which are denoted by the red markers in Fig. 3. The observations in Fig. 3 can be summarized as follows.

- For wind direction of 0°: (1) Figs. 3 a and c show that uplift for buildings 1-12 (H/B=0.25 to 2) are about the same, indicating insensitivity to the geometry for these cases. (2) For buildings 19-30 (H/B=2 to 12), the uplift is distinctly varied with building configuration, in a way that indicates dependence on breadth. (3) For buildings 13-18 (H/B=1 to 4), the variation with building configuration is not as distinct as for the higher buildings (No. 19-30), but shows a more obvious tendency than the lower buildings (No. 1-12). The ASCE 7 provisions envelop these, quite conservatively.
- For wind direction of 90°: (1) The uplift has a monotonic tendency with building configuration, which is related to the condition of flow reattachment as a function of length, L. (2) The provisions in Chapter 27 again capture these conservatively (safely), but do not match the trends in the measured data. As an example of how we are examining modifications, we re-calculated the design wind loads using breadth, B, replacing roof height, H. The newly updated design loads better capture the trend with building configuration for wind direction of 90°, as the blue markers show. (Such a recommendation is not final, but indicates how we relate geometric parameters to the resulting flow patterns and aerodynamics, to better capture the functional variations in a simple way.)

Fig. 4 further plots the mean and peak uplift versus the geometric parameter, L/B. The red line indicates the existing provisions but with B replacing H. We can conclude that for the buildings with H/W=8 and 12, B/L (or L/B) is the better parameter to capture the tendencies in uplift. We would define this as the boundary defining a “high-rise building” (H/B > 4). In contrst, buildings with H/W=1 to 2 for the load case of 0° with H/B range 1-2, can be defined as “mid-rise buildings”. There is, of course, transitional cases between these two bounds. Detailed explanations will be provided in subsequent reporting, which include all building configurations.

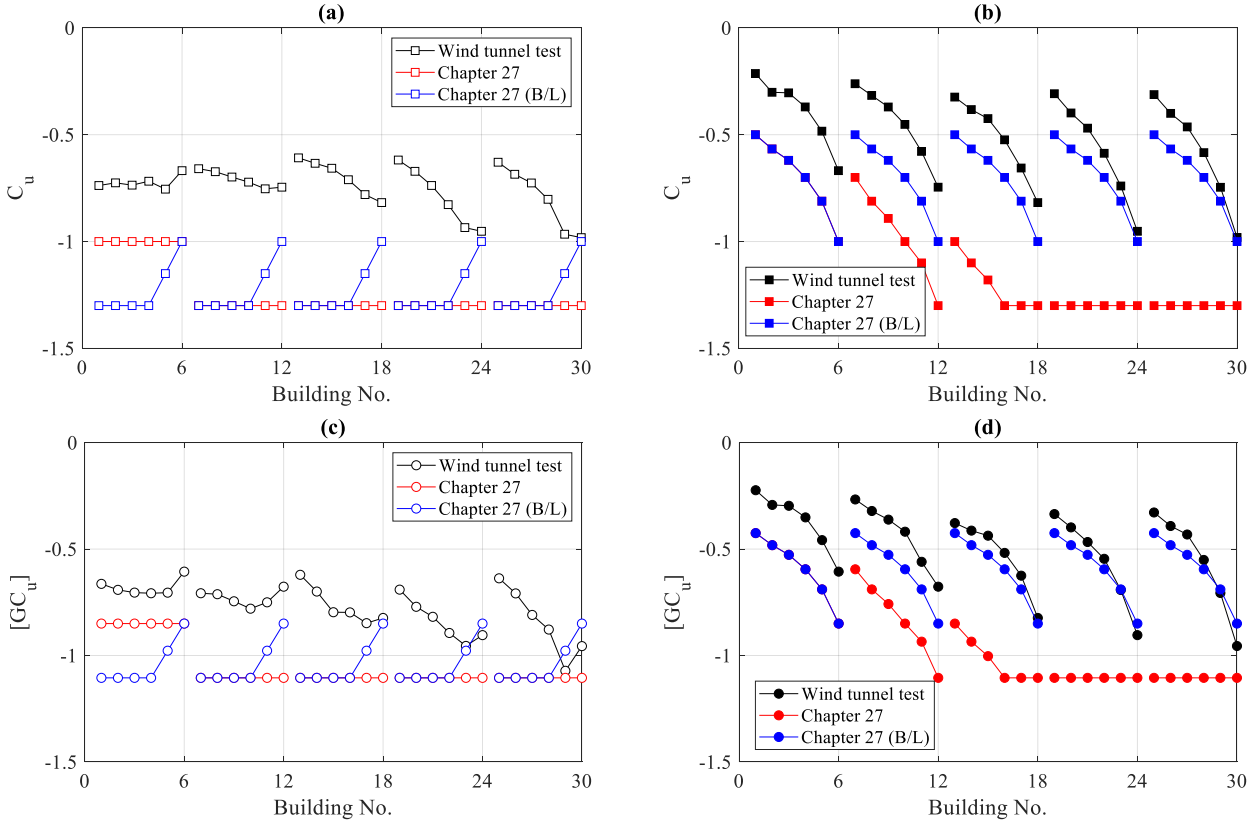

Fig. 3 Mean and peak uplift coefficients: (a) mean uplift coefficients for wind direction=0°; (b) mean uplift coefficients for wind direction=90°; (c) peak uplift coefficients for wind direction=0°; (d) peak uplift coefficients for wind direction=90°

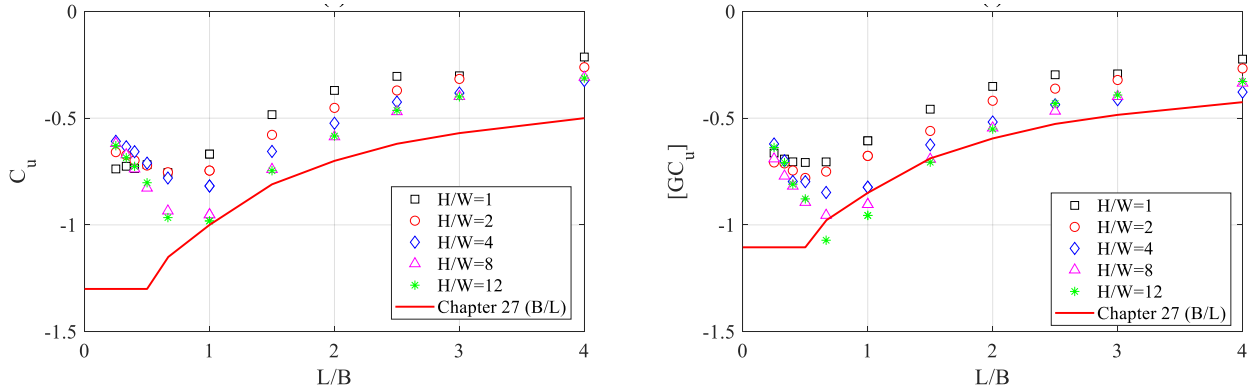

Fig. 4 Mean and peak uplift coefficients versus L/B: (a) mean uplift coefficients versus L/B; (b) peak uplift coefficients versus L/B

3.2 Base shear

Fig. 5 presents the mean and peak base shear coefficients for the two wind directions. The provisions of Chapter 27 capture the trend with building configurations for a wind direction of 90°. However, while the mean coefficients are higher than the measured data, the peak values match well, indicating the provided gust-effect factor of 0.85 (for rigid buildings) in Chapter 27 is not accurate. Additionally, the 0° case indicates a different trend with building configuration when compared to the data for 90°. Again, the gust effect factor appears to be the primary issue. As for uplift, Fig. 6 provides the relationship of mean and peak base shear as a function of the geometric parameter, L/B. It is observed that for many configurations, the provisions of Chapter 27 are reasonable, although there are some issues when L/B < 1 for high-rise buildings. In addition, the data for buildings with H/W=8 collapse well with those with H/W=12. For the mid-rise buildings, the base shear coefficients are reduced, further indicating the mid-rise building and high-rise building definition. We will discuss these concepts in subsequent analysis and reporting.

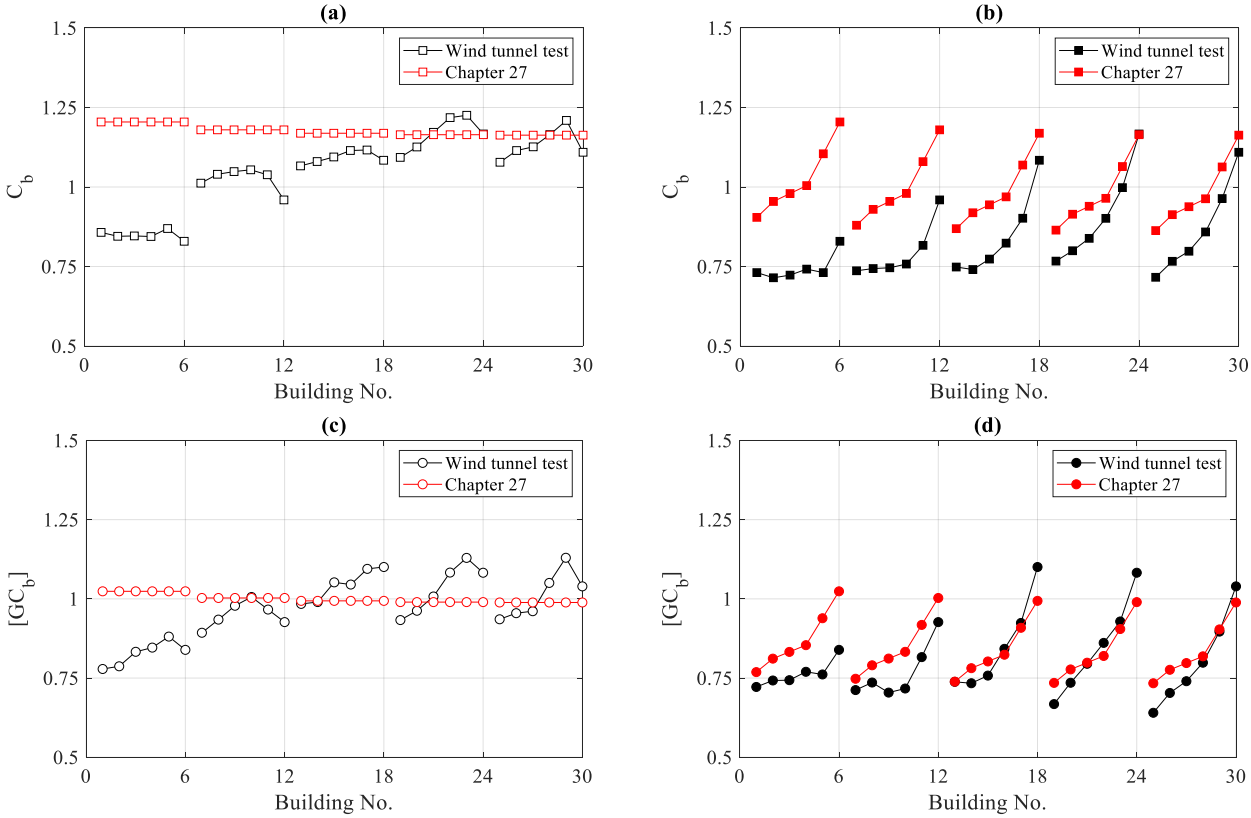

Fig. 5 Mean and peak base shear coefficients: (a) mean base shear coefficients for wind direction=0°; (b) mean base shear coefficients for wind direction=90°; (c) peak base shear coefficients for wind direction=0°; (d) peak base shear coefficients for wind direction=90°

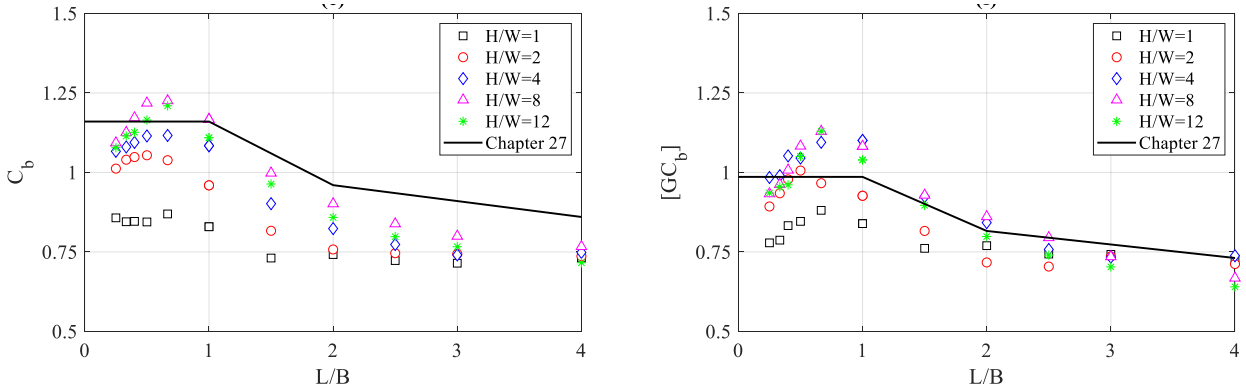

Fig. 6 Mean and peak base shear coefficients versus L/B: (a) mean base shear coefficients versus L/B; (b) peak base shear coefficients versus L/B

4. CONCLUSIONS

Wind tunnel aerodynamic data were obtained for mid- and high-rise buildings to augment existing databases for low-rise and high-rise buildings. These data are being compared with the current provision of Chapter 27 in ASCE 7-16, in combination with the other data. This report provides initial analysis of the data with respect to overall loads (roof uplift and base shear). Further recommendation on Chapter 27 for wall loads and gust-effect factor will be given in the subsequent reporting where the complete database will be analyzed.

5. REFERENCES

Akins, R.E., Peterka, J.A. and Cermak, J.E., 1977. Mean force and moment coefficients for buildings in turbulent boundary layers. Journal of Wind Engineering and Industrial Aerodynamics, 2(3), pp.195-209.

Ho, T.C.E., Surry, D., Morrish, D., Kopp, G.A., 2005, The UWO contribution to the NIST aerodynamic database for wind loads on low buildings: Part 1. Archiving format and basic aerodynamic data., Journal of Wind Engineering and Industrial Aerodynamics, 93, 1-30.

Liu, Y., Kopp, G.A. and Chen, S.F., 2019. Effects of plan dimensions on gust wind loads for high-rise buildings. Journal of Wind Engineering and Industrial Aerodynamics, 194, p.103980.